

Metal-as-insulation variant of no-insulation HTS winding technique: pancake tests under high background magnetic field and high current at 4.2 K

T Lécrevisse^{1,4} , A Badel², T Benkel^{2,3}, X Chaud³, P Fazilleau¹ and P Tixador²

¹ CEA, Université Paris-Saclay, F-91191 Gif-sur-Yvette, France

² Université Grenoble Alpes, CNRS, G2ELab, Institut Néel, F-38042 Grenoble, France

³ CNRS, Laboratoire National des Champs Magnétiques Intenses (LNCMI), Université Grenoble Alpes, F-38042 Grenoble, France

E-mail: thibault.lecrevisse@cea.fr

Received 23 November 2017, revised 2 March 2018

Accepted for publication 7 March 2018

Published 4 April 2018



Abstract

In the framework of a project aiming at fabricating a 10 T high temperature superconducting (HTS) insert to operate in a 20 T background field, we are investigating the behavior of pancakes consisting of a REBCO HTS tape co-wound with a stainless steel tape (metal-as-insulation (MI) coil). The MI winding is inducing a significant turn-to-turn electrical resistance which helps to reduce the charging time delay. Despite this resistance, the self-protection feature of no-insulation coils is still enabled, thanks to the voltage limit of the power supply. We have built a single pancake coil representative of the pancake that will be used in the insert and performed tests under very high background magnetic field. Our coil experienced over 100 heater induced quenches without a measureable increase of its internal resistance. We have gathered stability and quench behavior data for magnetic fields and engineering current densities (j_e) in the range of 0–17 T and 0–635 A mm⁻² respectively. We also present our very first experiments on the insert/outsert interaction in the case of a resistive magnet fault. We show that if self-protection of the MI winding is really effective in the case of a MI coil quench, a major issue comes from the outsert fault which induces a huge current inside the MI coil.

Keywords: REBCO coil, no-insulation coil, metal-as-insulation coil, HTS insert, quench protection, magnet interaction, NI coil

(Some figures may appear in colour only in the online journal)

1. Introduction

Our ongoing work on the French project NOUGAT to fabricate a 10 T high temperature superconducting (HTS) insert intended to operate in a 20 T background field needs to validate high field HTS insert technologies [1–3]. The key feature of this project is an insert test program in a 20 T resistive background field from an existing magnet at the Grenoble National High Field Magnet

Laboratory (LNCMI-G) to pave the way towards a 30 T all superconducting user magnet. The geometric constrains are to place the insert in a 125 mm cold bore cryostat and to keep an insert inner diameter of 40 mm in order to obtain a user magnet, i.e. enough room to set up an experiment. As quench detection and protection are still at stake, it is currently very complicated to have a classical insulated and protected HTS magnet. Such magnets would need an active protection with very low threshold detection and very high quench heater power [4]. That is why the recent development of a no-insulation (NI) REBCO

⁴ Author to whom any correspondence should be addressed.

magnet seems to be so promising [5–10]. It was proposed in 2016 an alternative of the NI winding consisting of co-wound non insulated HTS and stainless steel tapes [11]. This winding technique was already proposed by Hahn *et al* in 2011 but for mechanical reasons (removing the soft insulating materials) [12]. We are proposing to use the mechanical reinforcement tape, which is needed in a very high field insert, to improve the main drawback of classical NI windings: the very long charging time delay. The main question to be answered here is about the self-protection of such metal-as-insulation (MI) winding. More recently a similar winding has been proposed [13, 14]; the metal cladding insulation (MCI) relies on surrounding the copper shunt layer by a μm range layer of stainless steel. Despite the improvement of the REBCO coil protection [13], the thickness of the stainless steel coating layer is not large enough to improve the mechanical behavior of a coil.

As a preliminary study we investigate in this paper the behavior of a MI pancake coil highly instrumented to monitor internal voltages during coil operation. In the first part we discuss the normal operating conditions in a liquid helium (LHe) bath. It is followed by the coil response to a local heat disturbance. Then we focus on the cases of MI coil fault. Finally we will present first and very unique measurements in case of resistive outsert fault. This aspect is in our opinion the most critical issue, which can happen in our final magnet. Although the main advantage of the NI-MI-MCI coil is the self-protection behavior with its low or medium turn-to-turn contact resistance, this finite turn-to-turn resistance is also a major drawback for the protection during a fast outsert discharge.

2. Experimental set-up

2.1. MI pancake coil

2.1.1. Coil parameters. The MI pancake coil is designed to be the same dimensions as a typical double pancake designed for the project. The pancake coil consists of two co-wound tapes: the superconducting tape SCS6050-AP-20 from SuperPower® and a Durnomag® alloy from Laminerie Matthey SA. Both tapes are 6 mm wide but 75 μm and 30 μm thick, respectively. The pancake coil has 238 turns and about 5.7 mm of over banding (OB), i.e. 192 turns of Durnomag®. This OB purpose is to reduce the global coil deformation, due to Laplace stresses, and keep the global SC tape strain below the limit of 0.4%. The main parameters of the coil are summarized in the table 1. The coil should be able to produce up to 2.39 T with a limiting current of 660 A in self-field (SF) and 2.10 T with the limiting current of 580 A in a 16 T background field (B_{ext}). A photograph of the pancake coil sample mounted on the probe is presented in figure 1.

2.1.2. Quench heaters. One goal of this sample coil is to study the stability and the quench behavior when a local heat deposition occurs. We imbedded three stainless steel heaters inside the winding as 3 mm wide and 30 μm thick Durnomag® tapes soldered with 30 μm thick and 2 mm wide current leads (CL). Heaters are surrounded by one layer of Kapton® tape for

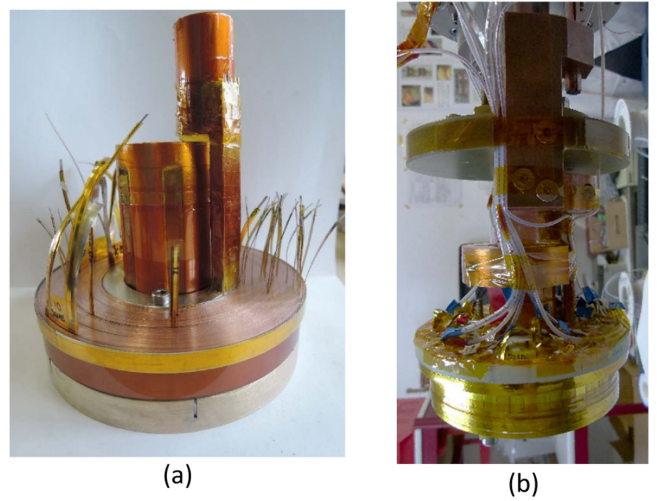


Figure 1. Photograph of the MI pancake coil (a) and mounted on the

Table 1. MI pancake coil main parameters.

Parameter	Unit	Value
Winding inner diameter (ID_w)	mm	60
Winding outer diameter (OD_w)	mm	110.2
Tape width (w_t)	mm	6
Over banding thickness (t_{OB})	mm	6.2
Winding turns number (Nbt)		238
Coil turn-to-turn resistance (R_c) (measured) ^a	$\text{m}\Omega$	9–12
Turn-to-turn characteristic resistance (R_{ct}) ^b	$\mu\Omega \text{ cm}^{-2}$	615–810
Coil constant (α_m)	mT A^{-1}	3.615
Coil self-inductance (L_{hts})	mH	5.832
Total SC tape length	m	64

^a Internal resistance is obtained from field delay after current ramp stop (τ_B) and self-inductance: $R_c = L_{\text{hts}}/\tau_B$.

^b R_{ct} is obtained from R_c following the formula in [15].

three electrical insulation. They are imbedded between two turns to maximize the amount of heat going in the winding. They are inserted between the 10th and 11th (H1), the 120th and 121th (H2) and the 224th and 225th (H3) turns. Heater H2 is 30 mm long divided in 2 parts of about 10–15 mm length. This heater set-up is to estimate the inner, middle and outer stability. By firing H2 the resistive grow can be accurately followed from the middle of the coil during a quench. The power of the heater was limited to about 30 W to avoid its burning. Typical heat pulse durations were between 50 and 100 ms.

2.1.3. Voltage taps. A total of 33 voltage taps made of 30 μm thick and about 1 mm wide Durnomag® ribbons have been imbedded in the winding in order to study the transient behavior of the coil. They were soldered on the Hastelloy® side of the SC tape to avoid any damage to the SC layer. 21 and 12 voltage taps are used for radial and azimuthal propagation follow up, respectively. They were positioned to study the propagation from the heater H2 position. The monitoring of these voltages is

also intended for benchmarking the quench code under development for NI-MI HTS magnets.

2.2. LNCMI-G 20 T test facility

2.2.1. The 170 mm 20 T resistive magnet. This experimental study was possible because of the 170 mm room temperature bore configuration of the high magnetic field resistive magnet available at LNCMI-G high field resistive magnet of the LNCMI-G M8 site. The magnet is a combination of two technologies developed at LNCMI: polyhelix and Bitter coils [16]. A total power of 20 MW is needed to produce 20 T and the facility power supplies (PS) are being modified to provide 36 MW in 2020 in the frame of the LNCMI-G hybrid project [17].

The probe is put in a 125 mm cold bore cryostat that was developed in 2012 for tests at variable temperature [18]. The CL have been designed to flow up to 1000 A under 20 T in the sample. Practically in our experiment current will be lower than 660 A (estimated SF critical current of the pancake coil). The probe itself is instrumented to monitor the sample temperature using cryogenics temperature sensors and a 336 Lakeshore controller and to supervise the CL resistance to avoid overload.

2.2.2. PS and control. The main PS for the pancake coil sample is a 6 V/1000 A PS designed and fabricated by LNCMI-G team. This PS operates with batteries in order to have a lower noise signal than conventional PS plugged on the 50 Hz network. Because of the CL resistance, the maximum voltage on the sample is about 4 V. This PS is controlled by a 10 V signal generated by our in-house LabVIEW program. This LabVIEW program has also been developed to read and record the global voltage and protection signals using Keithley nanovoltmeters 2182 A. Based on a threshold voltage detection higher than 100 mV for the MI pancake coil, it eventually forces whether the PS to shut-down or the current to ramp down according to a specified rate.

2.2.3. Data recording system. All signals are recorded through a National Instrument cDAQ-9178 Chassis [19] comprising eight modules. We chose the eight modules to be able to monitor different signals levels: one NI9238 with ± 0.5 V range for Hall probes and shunts signals, five NI9239 with ± 10 V range for coil and quench parts signals and two NI9229 modules with ± 60 V range for heaters, and global coil signals (half and whole coil). The data acquisition was performed at 1 kHz sampling and is increased up to 5 kHz sampling for a short time after the heat pulse. The sampling value is determined with a LabVIEW program.

3. Experimental results

3.1. Working conditions

3.1.1. Designed and working currents. It is of great interest to know the SC operating possibilities of the coil sample. The

classical way to do is to test the coil up to the critical current for increasing background magnetic field. We can do it easily because of MI technology and self-protection. Nevertheless due to the calculated high current in SF operation (660 A corresponding to 1050 A mm^{-2} and 1470 A mm^{-2} respectively for the stainless steel or for the SC tape section only), we chose to test up to 400 A in SF and then began to increase the external magnetic field. This sequence was chosen to avoid any burning in case of a limitation of the self-protection with very high current density. Unfortunately an outsert fault (very fast discharge of the outsert leading to very high induced current in the SC insert) damaged the CL connections and all following tests have been limited to 250–350 A depending on the background magnetic field. Limiting current or maximal test current are summarized in figure 2. The blue lines are the calculated critical current (dashed is 60% of I_c) at 4.2 K of the pancake coil using the critical surface fit from [20] and an in-house calculation algorithm with the CAST3M FEM software [21]. Empty symbols are the quench currents (black squares) or the maximal test currents (red circles). The red plain circles are the two maximal test currents before the first outsert fault. We only went up to 60% of the theoretical limit (I_{theo}) in SF before any damage. During this test no resistances were measurable inside the pancake coil and the internal and external CL resistances were respectively $460 \text{ n}\Omega$ and $215 \text{ n}\Omega$, including the joints between the coil and the CL.

3.1.2. Local perturbation. The HTS materials outperform their LTS counterpart when considering the stability against local perturbation which is of great interest for a user magnet. Indeed in such a magnet the quench has to be minimized to improve the safety and reliability of the installation. Thanks to the heater embedded within the MI coil, we were able to induce a quench and follow its development from the middle part of the coil. Because of the high thermal stability of the REBCO coil and especially the MI type coil, no quench was performed at a current lower than 150 A to avoid overheating of the heater. As the heat dissipation inside the coolant and the winding depends on heating time, heat pulse durations were near or shorter than 100 ms. In this part we are talking about quench energy (Q_q) and not minimum quench energy as it is a concept of a very local heat deposited instantly. In our case heat energy is deposited on a 30 mm^2 area in less than 110 ms. Figure 3 presents the quench energy versus the background field (a) and the coil current (b). All heating energies below the minimum value are followed by a recovery and all heating energies higher than the maximum value are followed by a thermal runaway. The real quench energy is between the two heating energies values. 250 A corresponds to about $0.38 I_c$ in SF and $0.42 I_c$ under 15 T background field. If Q_q decreases with increasing B_{ext} , this tendency also depends on the time deposition and has to be carefully studied. The increasing Q_q at 12 T is due to a longer heating time. The most important is the very high stability at high field (more than 1 J in a 30 mm^2 area) which is slightly lower at 16 T than at 8 T for similar heating time. Comparison

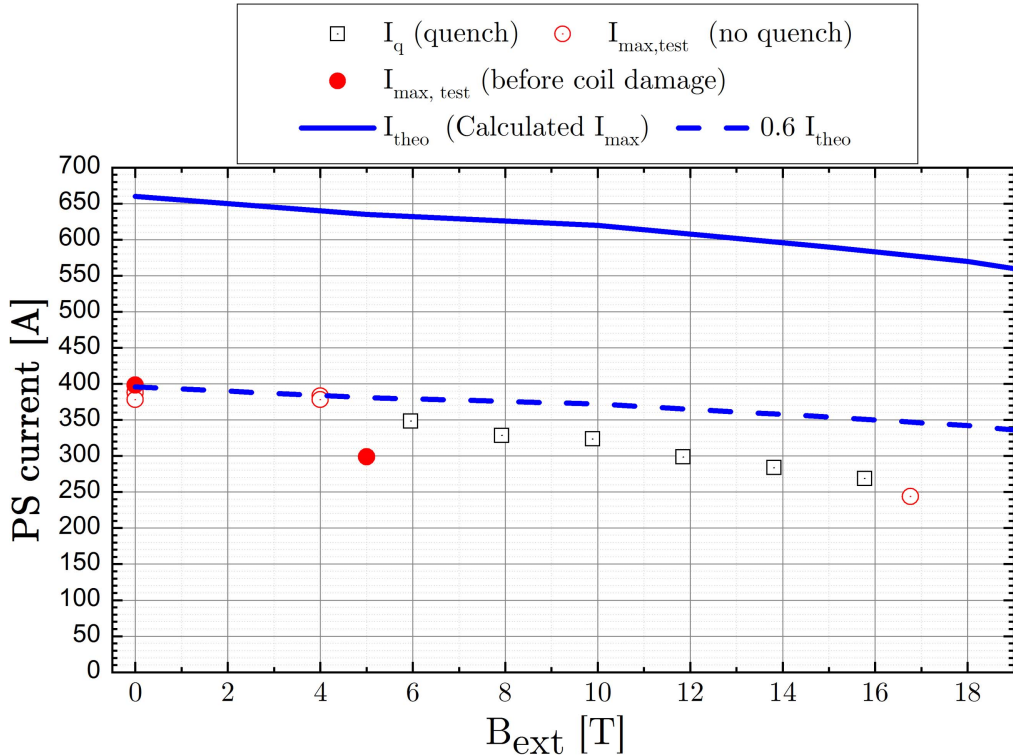


Figure 2. Power supply (PS) current versus background field. Empty black squares and red circles are respectively following or not by a quench. Plain red circles are maximal currents before damages and lines are calculated limits.

of quench energy with results obtained for insulated or NI REBCO is complicated as the experimental set-up and range study is unique. Nevertheless quench energy of near or above a Joule have been reported previously for insulated pancake coils [22, 23], but this value strongly depends on the cooling effect and computations result in a few tens of mJ. Some experimental measurements have been performed on MCI pancake coils by Kim *et al* [13]. Conditions were similar to our experiment (15 T at 4.2 K and 600 A mm⁻² inside the winding) and energy to quench the pancake coil went from 9 to 32 J, which is 5–20 times higher than our measurement. Tapes architecture and experimental set-up are different in our experiment compared to the experiment in [13]. Our sample consist of a co-winding of SC and SS tape but their sample is only a winding of a SC tape surrounded by a SS layer. Also the way to deposit the local heat is different (heater power and position) which can affect the heat proportion deposited inside the winding and in the coolant or structure. All those points can explain the difference in the quench energies we found and they measured.

3.1.3. MI HTS coil field generation. If we need a very stable magnet against local perturbation, we also need to have a known and stable field generation. This is needed to have a reliable and reproducible running behavior. If the field of a NI coil is rapidly modified with a small perturbation and could change with time due to copper layer surface oxidation (change of the turn-to-turn contact resistance), we expect the MI coil magnetic field generation to be more constant. We have then investigated two

aspects: the magnetic field generation tests after tests and the field generation during the ramping.

3.1.3.1. MI coil field generation over the tests. Our pancake coil endured many quenches and outsert faults. Each outsert fault inevitably induced local or area damages. In the case of classical insulated pancake, it would probably have locally burnt the SC tape in many locations inside the coil. The MI coil got damaged mainly because of very high induced current and following mechanical overstresses. Despite the damages due to extreme fault conditions which should significantly reduce the produced magnetic field, the MI pancake coil is still able to generate a magnetic field with nearly the same behavior as a classical insulated coil and the self-protection of a NI coil in case of a locally induced quench.

Figure 4 presents the magnet constant ratio (a view of the generated magnetic field normalized by the calculated value) in SF of our pancake coil before and after the first outsert fault. Magnet constant ranges between 3.56 and 3.68 mT A⁻¹. It is to be compared with the calculated value of 3.62 mT A⁻¹. The low influence of the outsert fault on the magnetic field generation confirmed a good resistance of the MI coil against such events. Nevertheless a reduction of 1.2% can be extracted from the data when comparing the first tests and lasts tests in the 2016 campaign. Our hypothesis is that some internal damages are certainly at the origin of the difference. Nevertheless this is not explaining all the measurements and some unexpected behavior can be seen. Sometimes the ratio is decreasing with increasing current (like the measurements

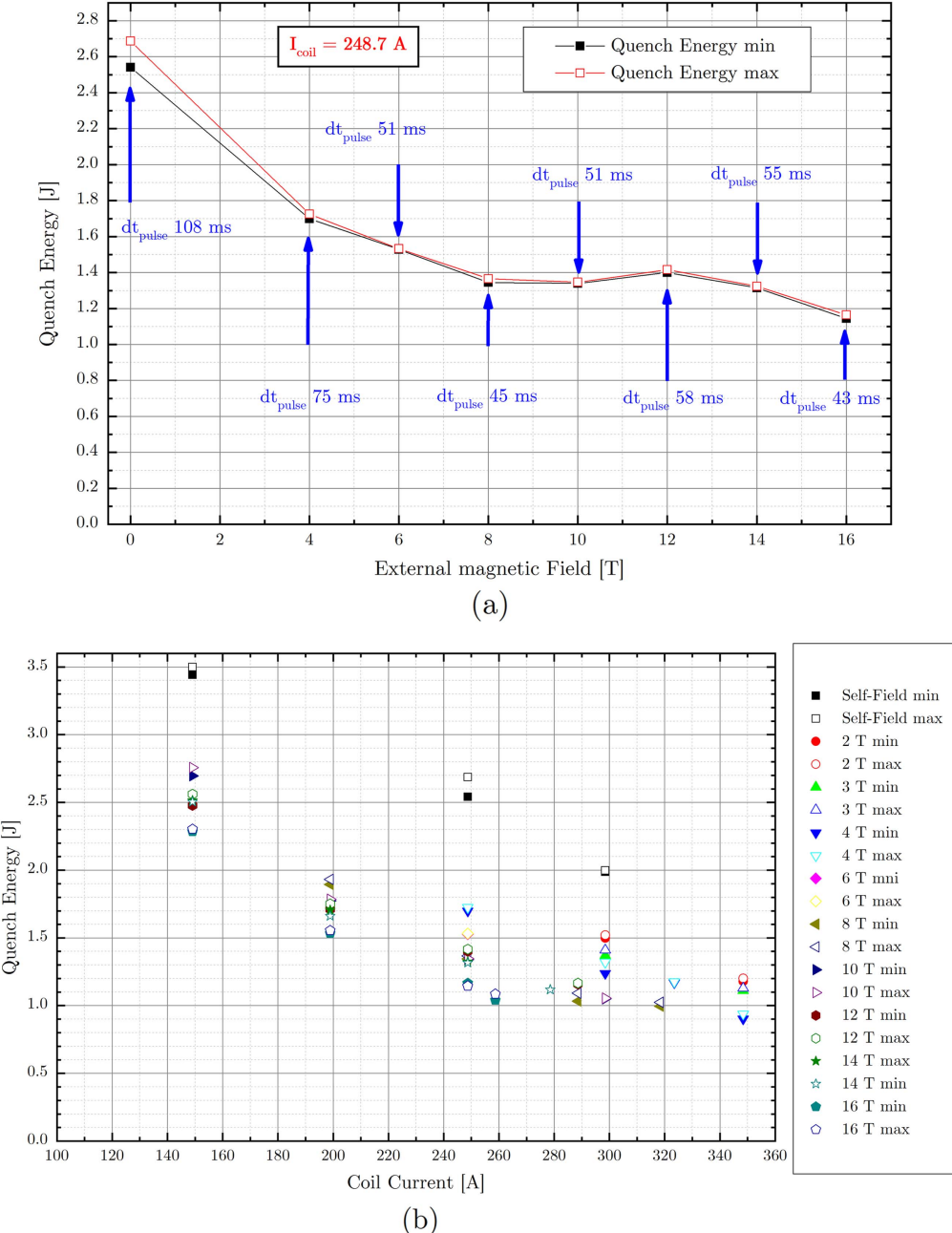


Figure 3. Quench energy versus external field (a) and coil current (b).

before the fault), sometimes the ratio is increasing and decreasing (like the measurements after the fault). Such behavior is probably due to the screening current induced field (SCIF) which is lowering the central field depending on the current ramping rate and duration. The only way to remove the SCIF is to increase the REBCO tape above the critical temperature and it was impossible to do it for the hundreds of tests we performed. The test sequence (previous tests—I, dI/dt , B—configuration) might also explain a part of the behavior similar to a ‘hysteresis’ on the magnetic field generation [24, 25].

Next data study is made on 2017 measurements as experimental set-up was improved as well as the data recording. As shown in figure 5, the normalized magnetic

field generation with the calculated value is fluctuating in less than 5% range over about 160 tests. As previously studied, the SCIF can affect the field generation (and so the magnet constant). Indeed the SCIF amplitude is increasing with increasing dB/dt and variation time. The change of the Hall probe set-up between 2016 and 2017 tests can explain the difference in magnetic field constant between figures 4 and 5. Again some differences and fluctuations can be seen between the tests. Such fluctuations are coming from the outer field influence, previous tests and also test current. In order to check any new damage which affect the field generation, the first tests and last tests can be compared as they are in SF. The final value of 3.573 mT A^{-1} is very similar to the 3.575 mT A^{-1} value at the beginning of the 2017 tests.

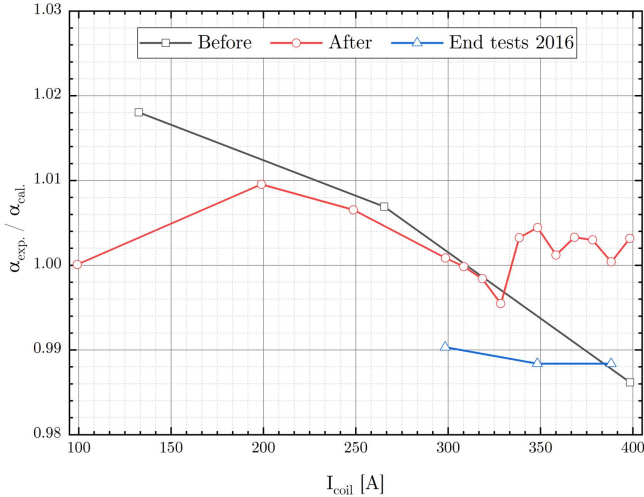


Figure 4. Magnet constant $\alpha_{\text{exp.}}/\alpha_{\text{cal.}}$ in self-field before, after the first outsert fault in 2016 and at the end of the 2016 tests.

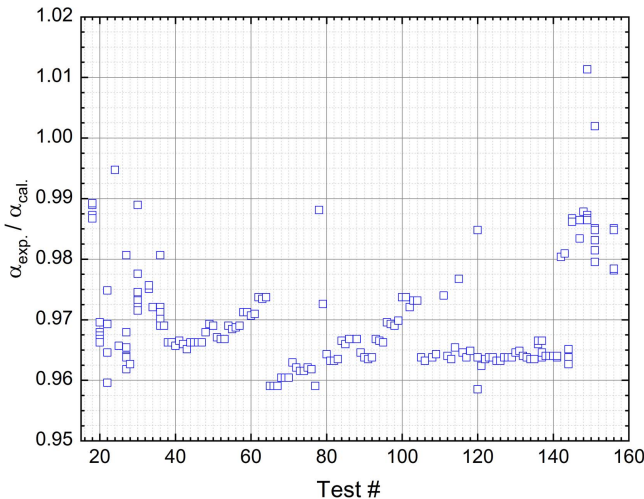


Figure 5. Normalized magnet constant $\alpha_{\text{exp.}}/\alpha_{\text{cal.}}$ during 2017 tests.

If the coil was significantly damaged when it was unwound (see section 3.3.4), on more than 3% of the total length, the magnetic field generation is affected in a very small range: about 1% of reduction. To conclude MI winding technique is very reliable against quench for the magnetic field and internal voltage generation.

3.1.3.2. Bypassing current during fast charge. Another aspect of the field generation is the possibility to ramp up the magnet very quickly, even near the current limit and with the expected field generation during current ramp. This is the main drawback of NI magnets and here some data are given on the influence of the current ramp up on the field generation during the fast charge of the magnet.

For this study the coil was charged up to 1 A lower than the quench current. The highest current ramp presented is the one without a coil thermal runaway. Higher current ramps have been tested but a quench occurs during the process.

A simple model of the MI coil is the same that for its NI counterpart: a resistance in parallel with an inductance [12].

Charging the coil with a higher dI/dt means a higher voltage and so more bypassing current. The magnetic field ratio according to the time, beginning at the end of the current ramp is shown for few current ramp values in figure 6. The Y-axis is also a good view of the current establishment inside the coil. Considering the 10 T case, bypassing current is about 1% at 20 A s^{-1} , 4% at 50 A s^{-1} and 4.5% at 60 A s^{-1} . It seems to be linear with the current ramp but presents a little change between 50 and 60 A s^{-1} . The behavior is the same under 16 T with a slightly lower slope. About 0.9% more current is bypassing at 16 T compared to 10 T with a current rate of 20 A s^{-1} . This difference might come from higher magnetic stresses at higher field which improves the contact between turns (lower the resistance) and, in consequence, increases the bypassing current. Also the variation of the materials electrical resistivity (ρ) with magnetic field could modify the internal resistance of the coil.

Even if the bypassing current is in the order of few percent, depending on the current ramp, the full magnetic field is reaching its target value shortly (few seconds) after the current ramp stops. This example shows the possibility to charge the coil very quickly and also the very good stability in LHe bath. Those results have to be correlated with the very good cooling efficiency of our pancake coil sample. No thermal runaway occurs even at 60 A s^{-1} in a 10 T background field and up to 99.6% of the quench current. Finally, the 2 tests at 60 A s^{-1} under 10 T shows the good reproducibility of the charging behavior.

3.2. HTS MI pancake coil fault

In our project, two faults can occur: the first is a fault (i.e. quench) of the HTS magnet. The second is a fault (fast discharge) of the outsert resistive magnet. The HTS quench is detailed in this section.

3.2.1. Quench and recovery behavior. In this study, several tests were performed to get the quench energy (Q_q) in many $(I_{\text{coil}}, B_{\text{ext}})$ configurations at 4.2 K in LHe bath. This allows us to present signals for an energy just below Q_q and for Q_q . One of the main results is the high magnetic field stability even with a significant voltage inside the coil. When looking at the beginning of the quench (see figure 7) and before the PS current drop, the magnetic field is nearly stable. It is only possible if the circulating current (which produces the central magnetic field) stays nearly constant (at least in average). This behavior shows the particularity of the MI pancake coil where the bypassing is very localized near the hot spot region or flowing azimuthally in the shunt layer and/or co-wound tape. It has also being reported for MCI pancake coil but at very low voltage [24]. Figure 8 presents an example of a quench test with a current of 260 A and a background magnetic field of 16 T. During this test several heat pulses were performed with increasing energy. No protection was implemented and the PS voltage limit was about 4 V. We will focus now on the recovery and the quench behavior during this test.

The recovery behavior is shown in figure 9 where only the last two pulses following by a recovery are presented. For

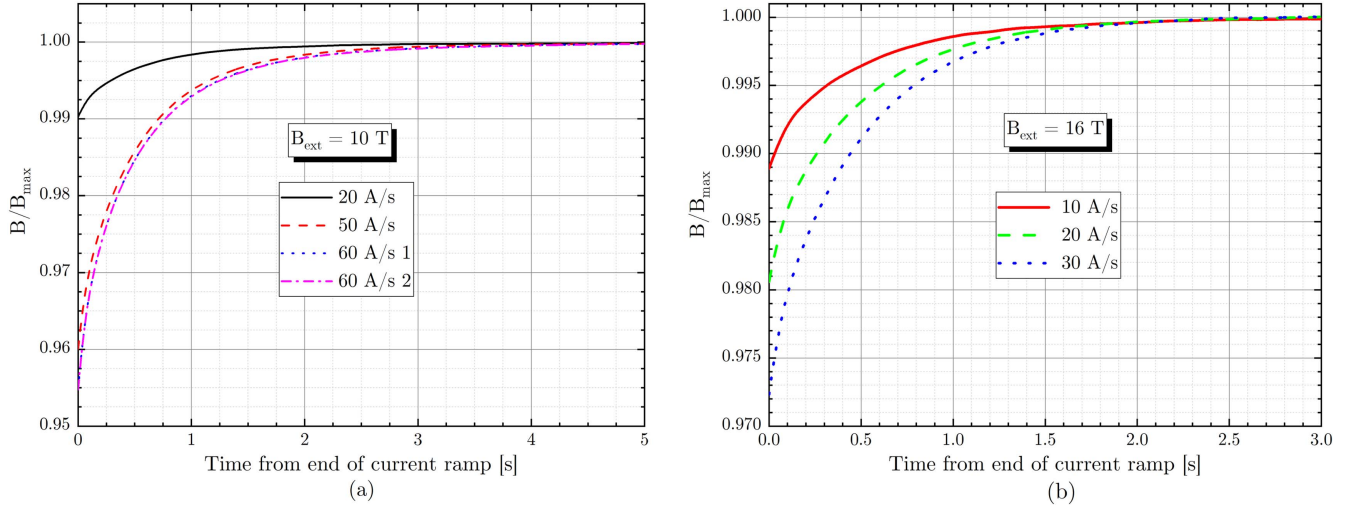


Figure 6. Current ramp up study at 10 T/397.4 A (a) and 16 T/257.4 A (b).

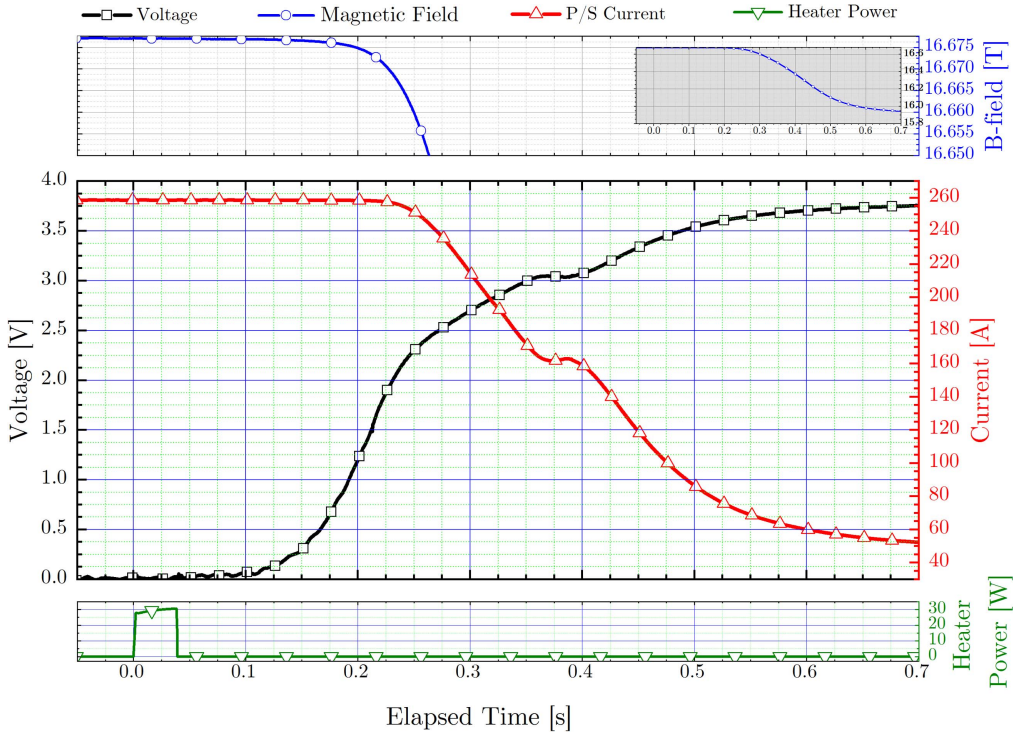
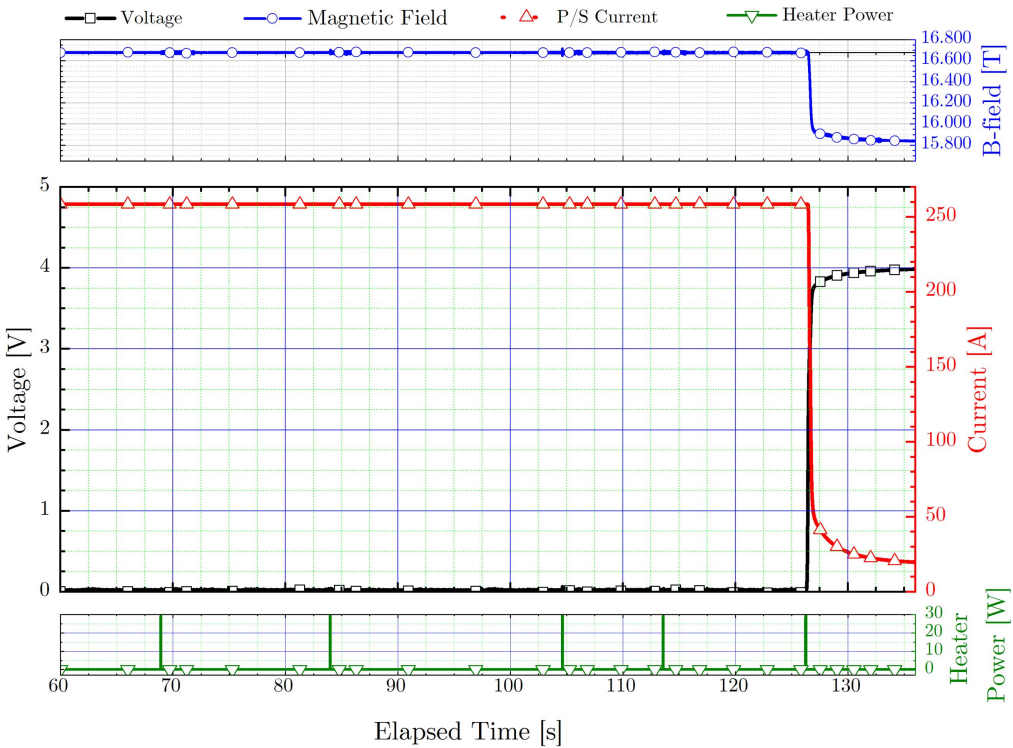
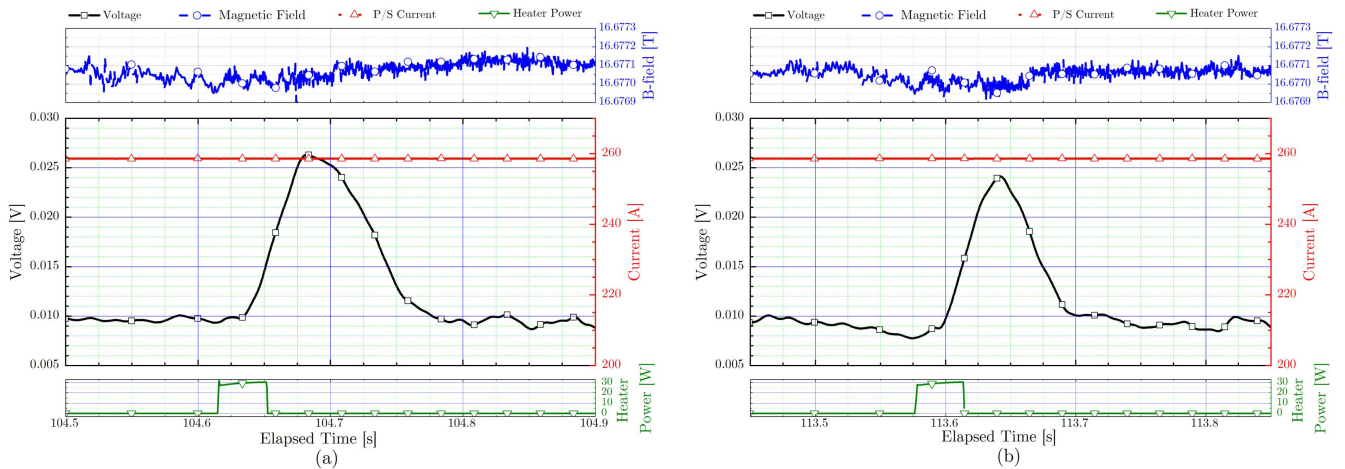


Figure 7. Global signals during quench at 260 A under 16 T background field.

a better comparison, both charts time ranges are 400 ms after the beginning of the heat pulse. The global signals of the coil show a very stable magnetic field stability with a voltage reaching more than 25 mV. At this time (104.75 s), the central magnetic field variation is lower than 2.5 Gauss (in the signal global fluctuation range). The noisy environment given by the 16 T resistive background magnetic field does not allow us to confirm the origin of the fluctuation (thermal perturbation or measurement accuracy). This stable magnetic field generation even with a significant voltage is to be compared with the NI counterpart. As bypassing current is much higher in a NI coil, the magnetic field drop significantly in case of an overcurrent or a local quench. A 6% field drop with a 25 mV end to end

coil voltage has been reported in [7]. For MI coils, two things might explain the field stability: no (or low) bypassing current, or a current azimuthally shared with the copper shunt layer and the co-wound SS tape. Also a compensation by adjacent turns (magnetic coupling between the quenched turns and the rest of the winding) can lower or cancel the magnetic field decay. The co-winding materials, which is directly in contact with the SC tape, also helps to reduce the hot spot temperature before the current begins to bypass through it.

The second aspect to be studied is the quench behavior of a MI coil. Although most research groups are stopping the test when a voltage is reaching a low threshold value (few tens of

**Figure 8.** Global signals at 260 A under 16 T.**Figure 9.** Recovery of a quench at 260 A and 16 T background field: third (a) and fourth (b) pulses.

μ V or mV in most cases) [13], here the self-protection aspect is studied when all detections are disconnected. A classical PS voltage limitation of about 4 V (set on the PS) is used and the global signals of the coil are presented in figure 7. The inset on the top chart represents the full scale of the magnetic field drop. The coil voltage increases quickly after about 100 ms, which is the time needed for the thermal runaway to occur. Despite the magnetic field is very stable at low voltage, the bypassing effect is clearly visible during a quench. The bypassing effect is less efficient on MI coils than on its NI counterparts for which over 15% magnetic field reduction has been reported with a terminal voltage lower than 1 mV [26]. Before the PS current begins to decrease, which occurs after about 225 ms (at this time the coil voltage is higher than

1.5 V), the magnetic field drop is about 6 mT ($<0.7\%$ of the produced magnetic field). After this time, both bypassing and current decay are working to discharge the magnet. Finally the current decreases to about 50 A at 700 ms (40 A at 1.5 s) and the coil voltage reaches about 3.75 V. The self-protection effect under strong magnetic field and high current density (over 410 A mm^{-2} and 575 A mm^{-2} in the whole winding or only in the REBCO tape, respectively) is effective in the case of an MI coil, even if the origin is different from a classical NI coil. In one hand, the high internal resistance of a MI coil limits the PS current (voltage limitation mode). The coil energy is discharged partially inside the HTS winding and inside the PS or the circuit protection components. In the other hand, the internal resistance (and terminal voltage) of a

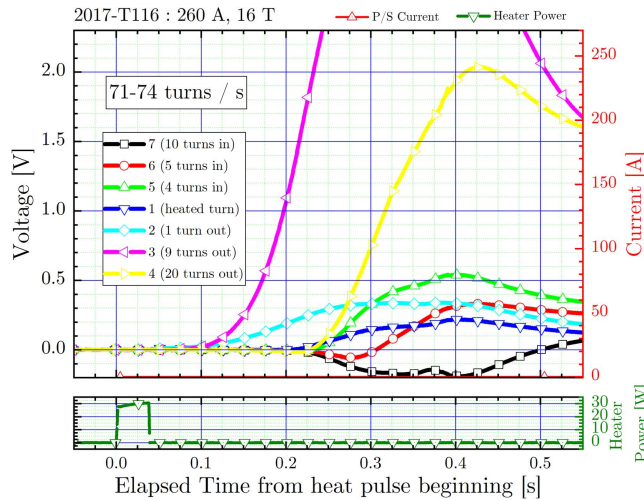


Figure 10. Radial quench propagation during a quench at 260 A under 16 T background field.

NI coil remains very low but the high proportion of current flowing through the turn-to-turn resistance avoids the hot spot overheating.

3.2.2. Quench velocity estimation. A magnet protection scheme needs a few accurate parameters. The quench propagation is one of the main parameters requested. The hot spot temperature is directly linked to the volume in which the stored energy is dissipated. The radial propagation inside a single pancake coil is studied here, which is a first step for understanding the behavior. The signals from azimuthal propagation are not really understandable because of bypassing effects and they are not presented in this paper. The details of the quench propagation on the 20–30 turns close to the heated turn are presented in figure 10. The ‘in’ and ‘out’ in the legend is for turns going inside (in) and outside (out) from the heated turn. The number before the parenthesis is for the order in the quench sequence (based on 50 mV threshold). The radial quench velocity (here between 71 and 74 turns s^{-1}) is to be carefully used. The PS current decays shortly after the beginning of the quench, which modifies the classical velocity measurement (supposed to be at constant current). Nevertheless the measurements are showing a very quick turn-to-turn propagation. A better turn-to-turn thermal contact (compared to classical insulated coil) and the magnetic coupling between turns manly explain this result. In this condition, the whole pancake is estimated to be quenched in less than 2 s. This radial quench velocity is greater than for the polyimide insulated pancake coils [22].

Figure 11 presents four other quench examples with the numbers before parenthesis which reflect the order to reach the threshold of 50 mV. The charts template is the same for a better comparison. Sometimes the first turns to reach the threshold are outward and sometimes inward. For all charts the test ID (year-ID) and configuration (I, B) are on the top left.

An estimation of the radial quench velocity (V_q) is presented in figure 12. The values presented in the chart are

the average values (of at least two tests). The quench velocity is plotted versus the PS current for different values of background magnetic field. As it was expected the higher is the current, the fast the quench propagates (lower thermal margin and higher heat generation). In the 10 T cases, V_q is six times larger when current is double (from 150 to 300 A). Now the quench velocity variation at fixed current is considered (figure 13), V_q is increasing with field but less than for current dependency (only a factor 1.2 between 8 and 16 T). Although the results are very interesting in terms of quench protection (estimation of the quenched volume), it has to be carefully used and compared with other experiments or coils. The coil was damaged at the very beginning of the tests. Even if it only has a small impact on the quench at ‘low’ current (damages are located inside and outside and the heater is in the middle), it still might slightly change when the current is close to the quench current. It also has to be noted that for some velocity value, the quench propagation is too small before the current decay and we had to use the data obtained after the beginning of the current decay. This leads to a pessimistic quench velocity. The quench velocity seems to be nearly linear with the current and exponential with the magnetic field. The fit in figure 13 use the model $V_0 * e^{\frac{B}{B_0}} + V_{of}$ with $V_0 = 1.566 \text{ turns } s^{-1}$, $B_0 = 6.608 \text{ T}$ and $V_{of} = 47.131 \text{ turns } s^{-1}$. The main purpose of such data is to give measurements to benchmark numerical model in the near future.

3.3. The major issue of (resistive) outsert fault

The MI winding technique is for many aspects very promising for application in high field magnets. Stability, reproducibility and self-protection have been experimentally proved for high magnetic field and high current conditions. Many high magnetic field applications plan to use HTS tapes as insert because of the risks and the high cost of HTS tape.

When the outsert is a LTS magnet, an outsert fault is a known event and the discharge is in most case a smooth event. This fault leads to a lower induced current inside the HTS insert [1] compared to results presented in this section. Depending on the current margin, this can quench the HTS magnet or not. The induced current should be estimated to be sure that the stresses are lower than the mechanical limit. On the contrary it is much challenging in the case of a resistive outsert like in our project. As time constant in case of a resistive magnet failure is very small (seconds or a few seconds) with a very high magnetic field variations (tens of $T \text{ s}^{-1}$ at the beginning). If a way to protect a classical insulated insert is to discharge and connect the magnet to a specific discharge resistance (to limit the voltage), this is more complicated for a NI or a MI coil as the internal resistance is working like a dump with a fixed value. In the next study an experimental ‘qualification’ of the outsert discharge is investigated as well as the interaction with the MI coil. A way to reduce the induced currents and their effects is to add an eddy current shield, as in the hybrid magnets, but this is not an option in our project because of the space limitation.

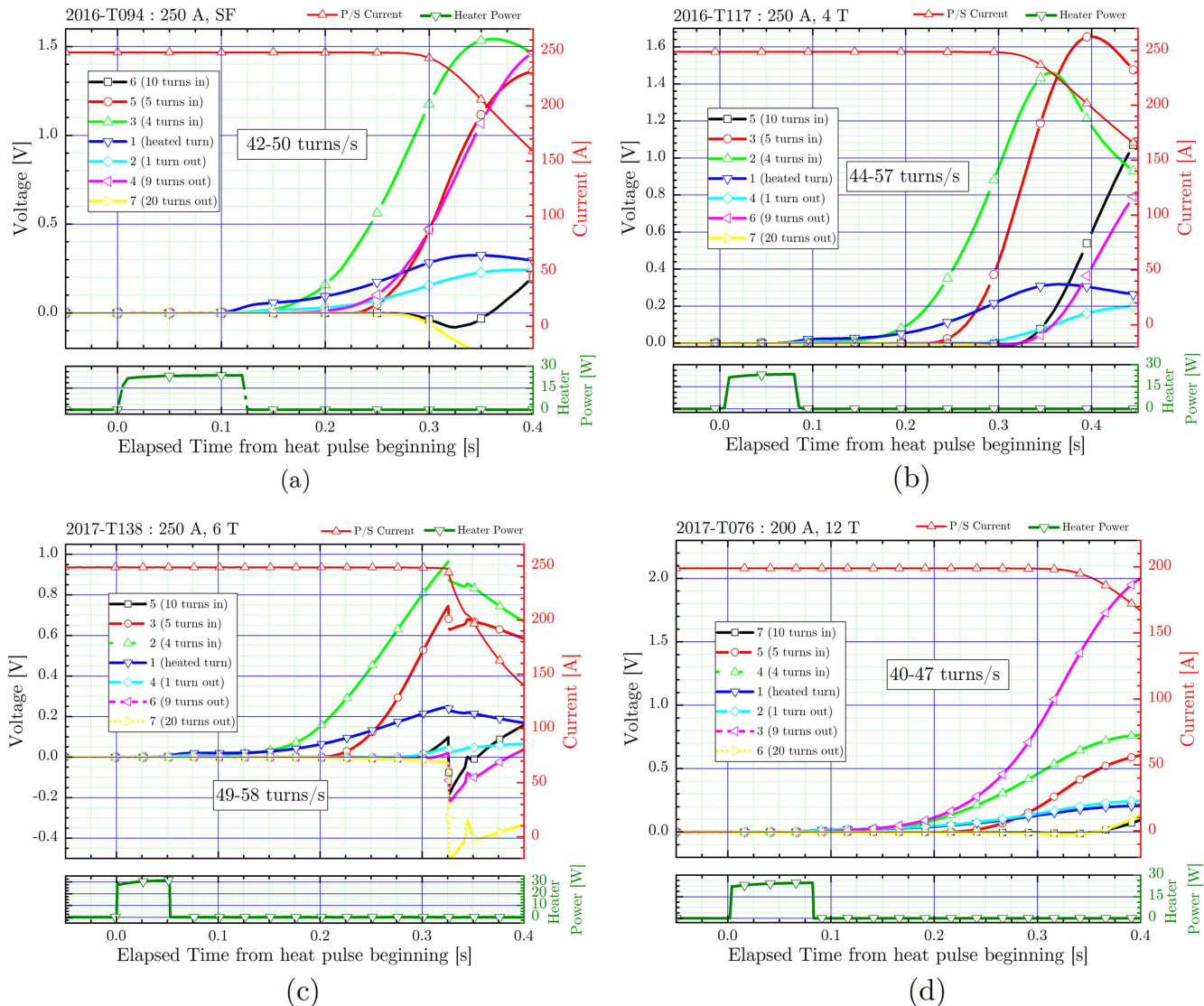


Figure 11. Examples of radial quench propagation for different test configurations.

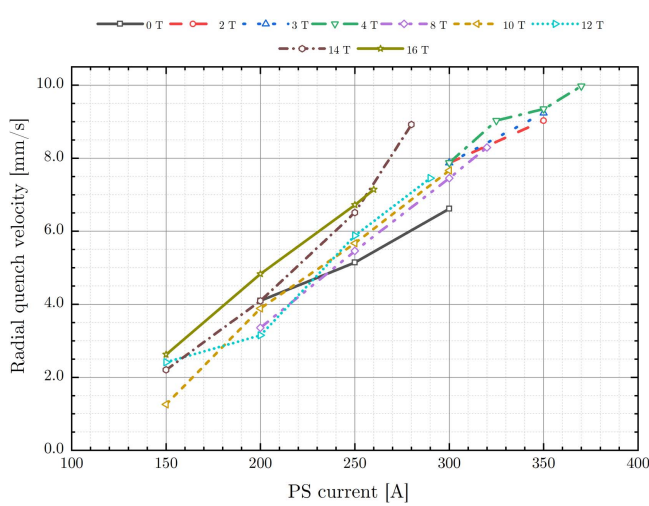


Figure 12. Quench radial velocity function of current and field.

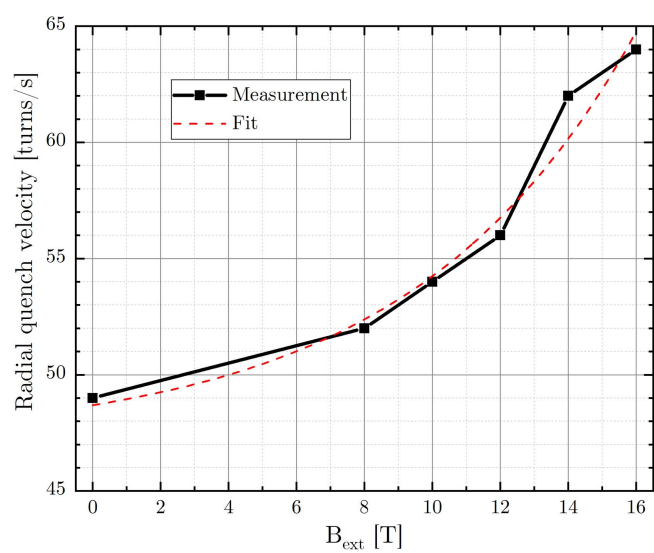


Figure 13. Estimated quench velocity versus field for 250 A.

Table 2. Main parameters of the resistive outsert magnet fault events.

Test ID	Fault origin	Initial B_{center} (T)	Discharge duration (s)	dB_{center}/dt max (T s^{-1})	dI_{shunt}/dt max (A s^{-1})	Remarks
2016-019	Power supply	8.60	5.0	-17.2	6479	During ramping B_{ext} from 5 to 10 T
2016-057	Power supply	10.38	4.9	-20.8	11792	With 100 A inside the HTS coil
2016-062	Power supply	3.21	5.5	-3.6	1176	From ramping B_{ext} from 0 to 10 T
2017-149	Transformer	17.50	6.0	-94.1	16000	During the HTS coil charging under 17 T

3.3.1. Outsert fault origin. In this experiment the fault are expected (manually caused) or unexpected (external reason). In the expected case, a fault is manually caused on one PS of the polyhelix or Bitter coils of the outsert magnet. In the case of the unexpected fault, either one PS or the main transformer were responsible. Without any doubt the unexpected events are the worst for the HTS magnet as the effects cannot be lowered in our experiment.

3.3.2. Explanations of the effects on the HTS insert. When a fault occurs on the background magnetic field, a very high current is magnetically induced inside the MI coil and this current is only limited by its own resistance and inductance. Because of the finite resistance between turns a part of the current is flowing radially when a voltage is applied at the terminals of the coil. This leads to a reduction of the magnetic field generation. From it we can estimate the bypassing current to be in the range of 10%–20% during the fault. The variation of resistance of the MI coil is also limited below the quench current (superconducting state). Once the quench current is reached, internal resistance of the HTS coil sharply increases. This resistance avoids the current to go at higher values for the rest of the outsert discharge. The challenge is here to estimate the heating and/or mechanical effect of the induced current on the coil winding.

3.3.3. Magnetic field compensation and induced current inside the MI pancake coil. In order to study the magnet field compensation and estimate the ‘average’ induced current, the magnet field constant (α) and the SF of the coil have to be known with accuracy. In 2016 we only measured the central magnetic field. During the first unexpected outsert fast discharge, the central magnetic field is recorded but without a precise measurement of the SF of the MI coil in case of an outsert magnetic field variation. After the incident, a second Hall probe has been added on the top of the sample for the 2017 tests. Unfortunately, the second Hall sensor has been unglued from its support during the main transformer fault when the resistive field was set at 17 T. Due to the loss of the second Hall probe signal, the end of the test sequence (study with additional dump resistor effect) was not properly recorded.

The main parameters of these unexpected resistive magnet faults are presented in the table 2. Although all of them are critical because of the high induced current (probably up to the maximum current of the coil, around 600 A), the last drop which corresponds to a fault of all PS at

the same time is the worst. As there are no active protections implemented in this experiment (no switch breaker to physically disconnect the PS and put a dump resistor in parallel with the pancake coil), the only things which is limiting the induced current is the HTS coil internal resistance.

Figures 14 and 15 are showing the signals during the outsert magnetic field drop. It is impossible to know exactly what happened inside the coil even with all the voltage taps embedded inside the winding. Only a global description can be made supposing the current is homogenous inside the coil. This assumption is far from the reality and only an accurate computation can give answers about the local effects.

Assuming the current is homogenous inside the MI coil, the global voltage and shunt current are presented in figure 14 where the inset shows the whole test signals. The pancake coil was charged up to about 200 A when the fault occurred. At this time, because of the freewheeling diode of the PS, the voltage of the coil reached nearly -7 V before the pancake coil quenched and then reached up to 3 V, which is limited by the PS voltage. The maximum circulating current reached about 690 A. Figure 15 shows more details on the induced current inside the magnet. Before the fault, the current measured on the shunt (empty black squares) and the current calculated from the SF (red circles) are similar. During the fault, the circulating current reached 690 A, but only 560 A produce magnetic field (with assumption of invariant magnetic constant). We might suppose that the 130 A remaining are bypassing the coil through the turn-to-turn resistance. At this time (307.73 s), the center magnetic field is about 16.44 T and the external magnetic field is nearly 14.26 T. It means that our magnet produced 2.18 T under the background field. The corresponding current is very similar to the FEM calculation (figure 2) computed before the experiment.

Now if we look at the mechanical aspect during this test, we can consider the peak current to be the higher stresses inside the magnet. Under this configuration (590 A/14.3 T), a peak azimuthal stresses are calculated to be about 650–720 MPa which corresponds to a pic strain on the REBCO tape of about 0.47%. The calculation is made using the CAST3M FEM software [21]. This is a conservative calculation as it does not consider the local current, which might be much higher, and still this strain reach almost the degradation strain limit of the tape (about 0.4%–0.45%). This explains, at least partially, why a consequent damage of the coil was observed when we unwound it.

3.3.4. Damage induced inside the MI pancake coil. It is complicated to fully investigate the coil damages only from the voltage signals which show a high damage on both CL connections. A slow increase of voltages is also observed inside the coil. Nevertheless, if the assumption of damages on the CL connections have been confirmed when the coil sample was dismantled, the damages on the SC tape were worse than expected inside the winding. Examples of damage seen during dismantling the coil are presented in figure 16. The pictures show a broken internal and external CL connections. The CL burning indicates a high temperature increase (over 700 K) and the delamination corresponds to strong sheer stresses. The local damage on more than 80 turns beginning from outside of the winding, which is visible on the pictures, was not expected using the signals (magnetic field and voltages) study; the damage is estimated to be about 2 cm per turns radially aligned. The absence of any coloration (burning part) near the heater is comforting meaning that the quench self-protection is efficient without overheating over the tens of quenches. The phenomena which might have damaged the coil is for now unknown. The mechanics seems to be the main reason, but it still need to be deeper investigated as it can be due to several reasons such as the peak hoop stresses or the torque stresses due to bypassing current are two of them.

4. Conclusion

The MI coil is a good and promising alternative to the conventional insulated or NI winding coil. It presents the same self-protection aspect against local hot spot than NI coils but it also improves its main drawback which is the time constant. Even if the critical current of the pancake could not be measured directly because of the first outsert fault which damaged the CL connections, the estimation during outsert fault gives a value near the calculated one.

The field generation is also stable and a coil charged at more than 50 A s^{-1} is possible when the coil is properly cooled down, and reproducible even with a target current near the limiting current of our sample. At 50 A s^{-1} the bypassing current is estimated to be only 4%–5%.

We also proved the self-protection behavior of the MI coil against a local hot spot and its high stability even at more than 400 A mm^{-2} under a 16 T background field. Nevertheless the self-protection origin seems to be different for a MI coil that for its NI counterpart; for a NI coil, the quench propagation is fast radially due to the absence of polyimide insulation (few tens of turns per second). Although the resistance of the NI coil stays quite low, MI's internal resistance increases quickly and the self-protection is the consequence of the PS voltage limitation. In less than a few hundred milliseconds, the voltage at the terminals of the MI pancake coil goes over a few volts and the PS current automatically decreases as the PS is going into a voltage limitation mode. There is no sign of internal voltage change after each quench and also no presence of burned or damaged part near the heater either.

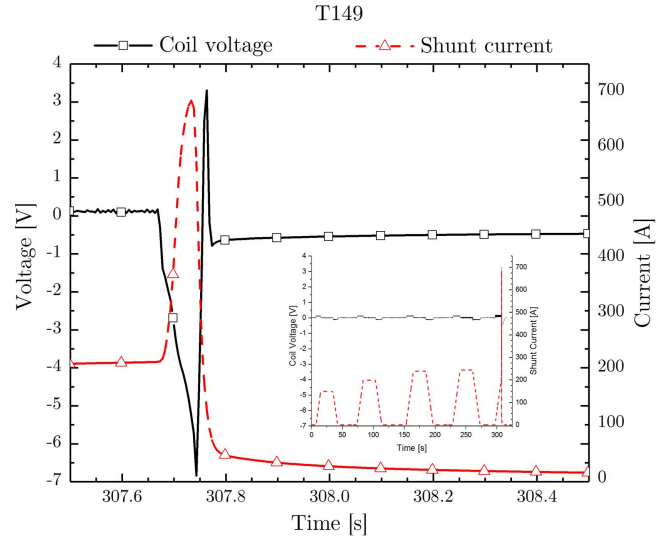


Figure 14. 17 T outsert fault—voltage and current.

One of the major issues, and probably the worst that the HTS insert can encounter, comes from the outsert/insert interaction. It is particularly risky when the outsert is a resistive magnet because of its discharge speed. The damages which have been seen after the outsert fault and the coil dismantling need to be carefully investigated to understand their origins.

A huge current is induced during the outsert fault and because of the electrical resistance between turns, there is no way to fully avoid it in a NI, partial insulation, MCI or MI magnet. The main work which needs to be done is to understand how such induced current can be lowered. We can expect that disconnecting the MI coil from the PS and its freewheeling protection diode could help to reduce the circulating current. Also the induced current has to be accurately estimated in order to include it in the fault scenario and mechanical design.

In the present study, all outsert faults induced a current inside the pancake MI coil up to its critical value and led to a quench. A first conservative approach would be to make a mechanical design considering the higher pancake critical current under the operating background field. Nevertheless even such a design will not reflect what happened locally inside the winding and a local huge high current can damage the magnet.

Acknowledgments

The authors acknowledge the support of the LNCMI-CNRS, member of the European Magnetic Field Laboratory (EMFL), and of the French National Research Agency (ANR) through the contract ANR-14-CE05-0005 (project NOUGAT).

The authors would like to thanks Eyub Yildiz from LNCMI-G for providing us the low noise sample power supply and the CEA and CNRS technicians for the realization of all pancake coil mechanical pieces.

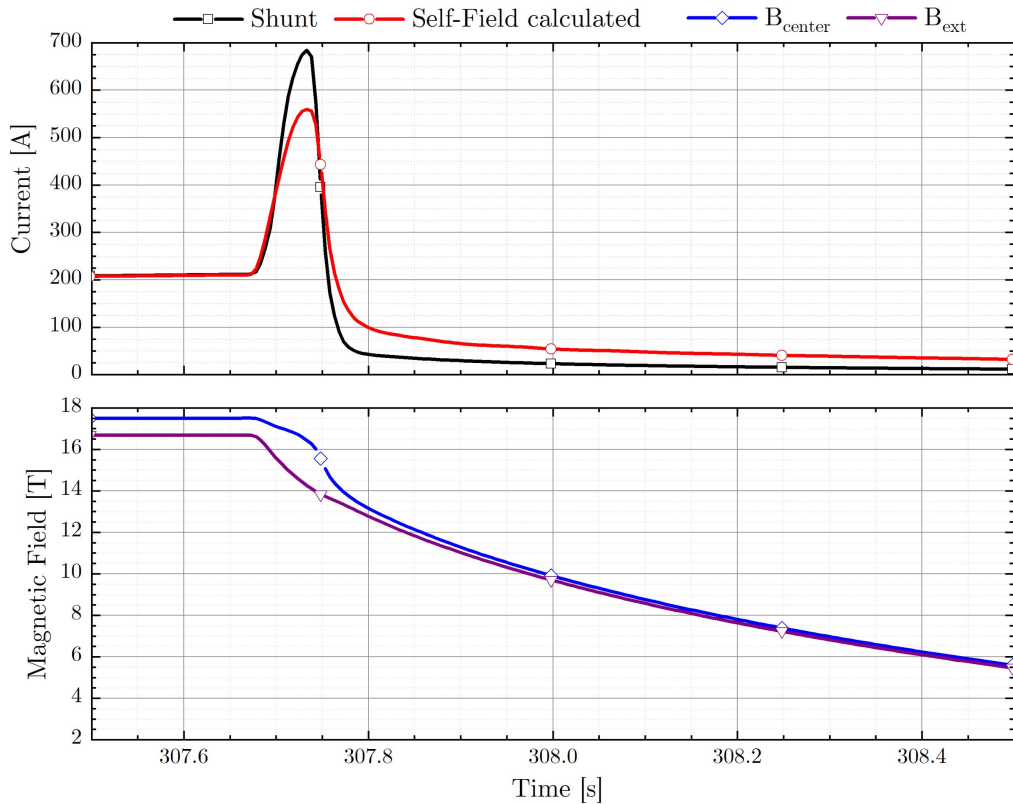


Figure 15. 17 T outsert fault—current and field.

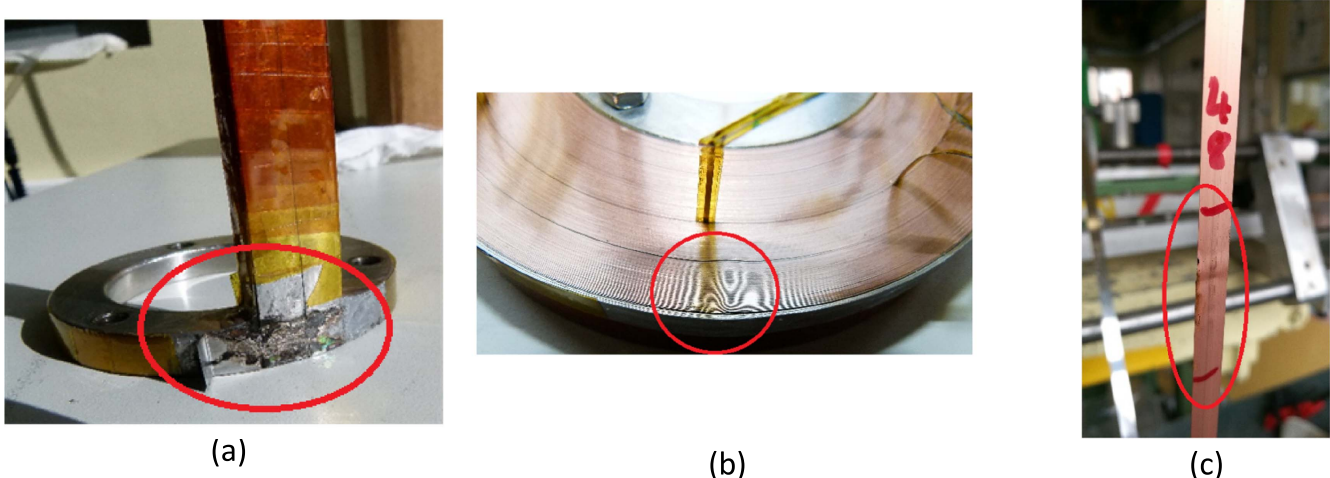


Figure 16. Damage of the coil (red circles): internal current lead (a), winding (b) and tape (turn 48 from outside, (c))

ORCID iDs

T Lécrevisse <https://orcid.org/0000-0001-6516-7600>

References

- [1] Benkel T, Richel N, Badel A, Chaud X, Lécrevisse T, Borgnolutti F, Fazilleau P, Takahashi K, Awaji S and Tixador P 2017 Preliminary tests and margin estimate for a REBCO insulated 10 T insert under high magnetic field *IEEE Trans. Appl. Supercond.* **27** 4602105
- [2] Benkel T, Miyoshi Y, Escamez G, Gonzales D, Chaud X, Badel A and Tixador P 2016 REBCO performance at high field with low incident angle and preliminary tests for a 10 T insert *IEEE Trans. Appl. Supercond.* **26** 4302705
- [3] Borgnolutti F, Badel A, Benkel T, Chaud X, Debray F, Fazilleau P, Lécrevisse T and Tixador P 2016 Design study of a 10 T REBCO insert solenoid *IEEE Trans. Appl. Supercond.* **26** 4600405
- [4] Weijers H W et al 2016 Progress in the development and construction of a 32 T superconducting magnet *IEEE Trans. Appl. Supercond.* **26** 4300807
- [5] Bascuñán J, Michael P, Hahn S, Lécrevisse T and Iwasa Y 2017 Construction and test results of coil 2 of a three-coil 800 MHz REBCO insert for the 1.3 GHz

- high-resolution NMR magnet *IEEE Trans. Appl. Supercond.* **27** 4300504
- [6] Bhattacharai K R, Kim K, Kim S, Lee S and Hahn S 2017 Quench analysis of a multiwidth no-insulation 7 T 78 mm REBCO magnet *IEEE Trans. Appl. Supercond.* **27** 4603505
- [7] Qu T, Michael P C, Bascuñán J, Lécrevisse T, Guan M, Hahn S and Iwasa Y 2017 Test of an 8.66 T REBCO insert coil with overbanding radial build for a 1.3 GHz LTS/HTS NMR magnet *IEEE Trans. Appl. Supercond.* **27** 4600605
- [8] Yoon S, Kim J, Cheon K, Lee H, Hahn S and Moon S-H 2016 26 T 35 mm all-GdBa₂Cu₃O_{7-x} multi-width no-insulation superconducting magnet *Supercond. Sci. Technol.* **29** 04LT04
- [9] Song J-B, Hahn S, Lécrevisse T, Voccio J, Bascuñán J and Iwasa Y 2015 Over-current quench test and self-protecting behavior of a 7 T/78 mm multi-width no-insulation REBCO magnet at 4.2 K *Supercond. Sci. Technol.* **28** 114001
- [10] Yoon S, Cheon K, Lee H, Moon S-H, Kim S-Y, Kim Y, Park S-H, Choi K and Hong G-W 2013 The performance of the conduction cooled 2G HTS magnet wound without turn to turn insulation generating 4.1 T in 102 mm bore *Physica C* **494** 242–5
- [11] Lécrevisse T and Iwasa Y 2016 A (RE)BCO pancake winding with metal-as-insulation *IEEE Trans. Appl. Supercond.* **26** 4700405
- [12] Hahn S, Park D K, Bascunan J and Iwasa Y 2011 HTS pancake coils without turn-to-turn insulation *IEEE Trans. Appl. Supercond.* **21** 1592–5
- [13] Kim K, Kim K, Bhattacharai K R, Radcliff K, Jang J Y, Hwang Y J, SangGap L, Yoon S and Hahn S 2017 Quench behavior of a no-insulation coil wound with stainless steel cladding REBCO tape at 4.2 K *Supercond. Sci. Technol.* **30** 075001
- [14] Kim J, Yoon S, Cheon K, Shin K H, Hahn S, Kim D L, Lee S, Lee H and Moon S H 2016 Effect of resistive metal cladding of HTS tape on the characteristic of no-insulation coil *IEEE Trans. Appl. Supercond.* **26** 4601906
- [15] Wang X, Hahn S, Kim Y, Bascuñán J, Voccio J, Lee H and Iwasa Y 2013 Turn-to-turn contact characteristics for an equivalent circuit model of no-insulation ReBCO pancake coil *Supercond. Sci. Technol.* **26** 035012
- [16] Debray F, Dumas J, Trophime C and Vidal N 2012 DC high field magnets at the LNCMI *IEEE Trans. Appl. Supercond.* **22** 4301804
- [17] Pugnat P et al 2016 Status of the 43 T hybrid magnet of LNCMI-Grenoble *IEEE Trans. Appl. Supercond.* **26** 4302405
- [18] Miyoshi Y et al 2013 HTS coil test facility in a large bore 20 T resistive magnet at LNCMI *IEEE Trans. Appl. Supercond.* **23** 9500204
- [19] National Instrument Specifications NI cDAQ™-9178 NI CompactDAQ Eight-Slot USB Chassis <http://ni.com/pdf/manuals/374046a.pdf>
- [20] Fleiter J and Ballarino A 2014 Parameterization of the critical surface of REBCO conductors from Fujikura *CERN internal Note* 2014-2024
- [21] Verpaux P, Charras T and Millard A 1988 Castem 2000 une approche moderne du calcul des structures *Calcul des Structures et Intelligence Artificielle* (Saint Etienne: Pluralis) pp 261–71
- [22] Miyoshi Y et al 2015 Performance tests of prototype high-field HTS coils in Grenoble *IEEE Trans. Appl. Supercond.* **25** 4600505
- [23] Lécrevisse T, Chaud X, Debray F, Devaux M, Fazilleau P, Juster F P, Miyoshi Y, Rey J M, Tixador P and Vincent B 2013 Quench propagation in YBCO pancake: experimental and computational results *IEEE Trans. Appl. Supercond.* **23** 4601805
- [24] Hwang Y J et al 2016 A study on mitigation of screening current induced field with a 3 T 100 mm conduction-cooled metallic cladding REBCO magnet *IEEE Trans. Appl. Supercond.* **27** 4701605
- [25] Yanagisawa Y, Nakagome H, Uglietti D, Kiyoshi T, Hu R, Takematsu T, Takao T, Takahashi M and Maeda H 2010 Effect of YBCO-coil shape on the screening current-induced magnetic field intensity *IEEE Trans. Appl. Supercond.* **20** 744–7
- [26] Zhang Z, Kim C H, Kim J G, Kviticovic J, Pamidi S, Zhang M, Li J and Yuan W 2017 An experimental investigation of the transient response of HTS non-insulation coil *J. Supercond. Noval Magn.* **30** 387–93